ELSEVIER

Journal of Nuclear Materials 257 (1998) 126–133

journal of nuclear materials

Investigation of structure and composition of surface oxides in a high chromium martensitic steel

I. Iordanova [a], K.S. Forcey [b,*], R. Harizanova [a], Y. Georgiev [c], M. Surtchev [a]

[a] *Department of Solid State Physics, University of Sofia, 5 Blvd.J.Bouchier, 1126 Sofia, Bulgaria*
[b] *Institute for Advanced Materials, Joint Research Centre, Ispra Establishment, TP800, I-21020 Ispra (VA), Italy*
[c] *Institute of Metallurgical Science, Bulgarian Academy of Science, 67 Shipchenski prohod, 1574 Sofia, Bulgaria*

Received 18 February 1998; accepted 21 May 1998

Abstract

An investigation has been carried out on the composition and thickness of the oxide films formed on the high chromium martensitic steel MANET under various oxidation conditions (ambient, 600°C in air and in hydrogen). X-ray diffraction methods were combined with ion beam techniques (Rutherford backscattering spectrometry (RBS) and nuclear reaction analysis (NRA)) to study the oxide films. In all cases the oxide layers were found to be highly enriched with Mn, a minor alloying component in the original steel. No evidence of the formation of pure Cr_2O_3 was found even in the samples oxidised under a low oxygen potential. © 1998 Elsevier Science B.V. All rights reserved.

1. Introduction

High chromium martensitic steels such as MANET have been proposed as structural materials for fusion reactors such as DEMO because of their resistance to radiation-induced void swelling and high temperature helium embrittlement [1]. However, such materials are considerably more permeable to tritium than austenitic steels such as 316L [2], which could prove a drawback for their use in fusion reactors. A number of authors have suggested the use of oxide layers to form surface permeation barriers on steels [3,4]. In particular, oxide layers grown under particular conditions (e.g. low oxygen potential) that promote the formation of Cr_2O_3, are thought to provide the most effective barriers to tritium. Although the presence of oxide layers is acknowledged to be important in determining the permeation of tritium through structural materials, little work has been carried out to determine in detail the oxide layers that form on high chromium martensitic steels under different oxidation conditions.

The present paper aims to investigate the chemical composition, structure and thickness of the surface oxide layers formed in martensitic stainless steel at ambient temperature; during annealing at 600°C in air; and during heating at 600°C in high purity hydrogen. The latter condition (low oxygen potential) was considered to be the most likely to form Cr_2O_3 layers. The methods chosen to investigate the oxide layers were X-ray diffraction for analysis of the crystal structures and accelerator-based methods (Rutherford backscattering (RBS) and nuclear reaction analysis (NRA)) for compositional and thickness measurements.

2. Oxidation processes

The tendency for a metal to oxidise is defined by the change of Gibbs free energy (ΔG) during oxidation. At temperatures normally encountered, this value is negative for the majority of metals, including iron, chromium and manganese, which results in a tendency to form oxides under many conditions. According to standard theories, the chromium content of the steel, because of its more negative ΔG for oxide formation, oxidises preferentially and makes the surface of the steel 'passive' by the formation of a surface oxide of Cr_2O_3, which protects the metal from further corrosion [5]. This view is an oversimplification and, in general, the oxide com-

* Corresponding author. Tel.: +39-332 786 225; fax: +39-332 785 013; e-mail: kevin.forcey@jrc.it.

0022-3115/98/$ – see front matter © 1998 Elsevier Science B.V. All rights reserved.
PII: S0022-3115(98)00446-2

position depends on the temperature, oxygen potential and time of exposure to the oxidising conditions. This follows from the fact that the oxidation process is controlled by the diffusion [6] of various metal ions each with a different starting concentration and ΔG of oxidation.

The diffusion characteristics of Cr and Fe are quite similar [7]. As a result it could be expected that chromium would form some complex (compound) surface oxides in which some of the positions of Cr cations will be occupied by iron and probably with other alloying elements. The possibility of formation of compound surface oxides in stainless steel is mentioned in Ref. [6]. One of the best known examples of such an oxide is the spinel $FeO{\cdot}Cr_2O_3$ which has a cubic structure. According to the usual view, oxidation of stainless steels contains three stages [8,9]: the nucleation stage, when all metal atoms on the surface can oxidise, forming a predominantly iron oxide; the transient stage, when the preferential oxidation of chromium leads to the formation of a dense, mainly chromium oxide layer at the metal/oxide interface; and the final stage, after the Cr_2O_3 layer has formed a passivating layer, when further oxidation occurs much more slowly by cation diffusion through this layer. It is considered that the outward diffusion of Cr ions can lead to the formation of the $FeO{\cdot}Cr_2O_3$ spinel between outer and inner oxide layers. Of course, the exact oxidation conditions determine the final oxide structure. In particular two parameters: oxygen potential and content of other alloying elements such as Mn are of interest in the present study. As the oxidation potential is reduced, the formation of Fe_2O_3 and other iron oxides is expected to be less favoured as compared to the growth of chromium and manganese oxides. Also, the presence of manganese in MANET, although at a low level may be very important. This is because as well as its relatively more negative ΔG for oxide formation, the diffusivity of Mn is very much greater (about 2 orders of magnitude) than that of Fe or Cr in Cr_2O_3 [10]. Thus, at high temperature when the diffusion process is activated, it could be expected that the surface oxide formed in martensitic stainless steel will be complex. For example, in Ref. [11] the formation of compound surface oxides $(Cr,Fe,Mn)_2O_3$ and $MnCr_2O_4$ spinels in various stainless steels with Cr content between 16–17% and with varying Mn content (0.4–1.59%) at 800–1100°C has been reported.

3. Material and experimental methods

3.1. Material

The investigated samples were discs of thickness 0.5 mm cut from a rod of 8 mm diameter. The rod is made of MANET I stainless steel with the following chemical composition (wt%): C-0.13; Cr-10.6; Ni-0.87, Mo-0.77; V-0.22; Nb-0.16; Si-0.37; Mn-0.82; S-0.004; P-0.005; B-0.0085; N-0.003; Al-0.054; Co-0.01; Cu-0.015; Zr-0.053; Fe-balance. Before cutting, the rod had been annealed to produce a fully martensitic structure following the established scheme: heating at 970°C for 2 h, austenizing at 1075°C for 0.5 h, quenching to room temperature and tempering at 750°C for 2 h. The disc-shaped samples were mechanically polished, finishing with 1 μm abrasive, cleaned and degreased, and then oxidised under various conditions as given in Table 1. All the samples except Nos. 1 (which was only exposed to ambient air) and 2 have been placed in a previously heated furnace, kept for the given times and then cooled in air. Sample 2 was put in a stainless steel chamber which before the annealing had been evacuated (to a pressure 10^{-4} Pa) and which was then filled with hydrogen taken from a palladium store to a constant pressure of 10^5 Pa. The annealing of this sample was carried out in three cycles. Each cycle involved the following: the temperature was increased to 600°C, maintained at this value for 7 h and then allowed to cool back to ambient temperature, thus repeating the heat treatment described in Ref. [12] after which a drastic decrease of diffusivity of hydrogen through MANET steel was observed, presumably due to the growth of a surface oxide film.

Table 1
Oxidation conditions

Sample no.	Temperature (°C)	Oxidising media	Oxidising time (h)
1	Ambient	Air	1450 (2 months)
2	600	Hydrogen	21.0
3	600	Air	0.17
4	600	Air	0.34
5	600	Air	2.0

3.2. Experimental techniques

X-ray diffraction qualitative phase analysis was performed using CuK_α and CoK_α radiation with the diffractometer in back reflection geometry. The spectra have been recorded by the step method, scanning through the 2θ angle (where θ is the Bragg angle) with steps of 0.05° and counting times of 200 s/step.

Two accelerator-based methods, namely: RBS of alpha-particles and O(d,p) NRA have been applied. The RBS method has been described in Ref. [13]. Briefly, the technique involves directing a beam of monoenergetic He^+ ions onto the surface to be studied and measuring the energy distribution of elastically backscattered alpha-particles resulting from collisions with atomic nuclei near the surface region of the sample. The energy of the backscattered alpha-particles depends both on masses of the scattering nuclei (metal and oxygen in the present

case) and also on the depth of the scattering events (since the particles lose energy while travelling through the material under analysis). Thus, analysis of RBS spectra can yield both compositional and depth information on the oxide films. The measurements were performed on the 3 MV Dynamitron accelerator of Birmingham University employing a 10 nA current of 2 MeV He^+ ions. The ion beam was held at normal incidence to the surface of the sample and the scattering angle was 150°. At the energy employed in the present work it was possible to investigate the sample to a depth of 1–2 μm (depending on target composition). The Rutherford scattering cross section of a target nucleus is proportional to the square of its atomic number and so RBS is a technique that is most sensitive to elements with high atomic numbers. For elements with low atomic numbers, NRA is a more sensitive technique. In the present work, a beam of deuterons was employed to induce the $^{16}O(d,p)^{17}O$ nuclear reaction in the surface of the samples. The number density of oxygen in the oxide and the thickness of the oxide film is obtained from the energy distribution of nuclear reaction products (in this case protons) resulting from the reaction between the incoming deuterons and the oxygen nuclei contained in the target material [13,14]. In this particular reaction protons are emitted at 2 discrete energies usually called the p_1 and p_0 groups (where the p_0 proton group are more energetic). The measurements were carried out using the Dynamitron accelerator with a 150 nA current of 1.1 MeV deuterons. The ion beam was held at normal incidence to the surface of the sample and the interaction angle was 150°. A computer program called SIMS [14] available at the Radiation Centre of Birmingham University was used to fit the experimental spectra and thus to obtain the compositional and depth information. The computer code produces simulated spectra for sample compositions which are input as a series of layers (starting at the outer surface and finishing with the substrate) each with fixed composition and thickness. Data analysis proceeds as follows: firstly a best estimate of the composition and thickness of the top few microns of the surface is made and used as input for the code. Then by comparison of real and simulated spectra, it is possible to make an improved estimate of the composition and layer structure and the simulation program is run again with the new input values. Thus, by an iterative process, a depth profile of the composition of the surface layer (or layers) is reached that produces the best fit between simulated and real spectra.

4. Results and discussion

The oxide films grown in the present experiment were all very much less than a micron in thickness and so the X-ray diffraction peaks corresponding to the surface film had a low intensity. Thus, in order to obtain higher precision in the results, all the samples were analysed by two different X-ray wavelengths, employing CuK_α and CoK_α radiation, allowing in principle two sets of data for each sample. The values obtained showed, in general, a good agreement, but the X-ray diffraction patterns registered using CuK_α radiation had a high background level due to X-ray fluorescence which partially obscured the relatively weak oxide peaks and in most cases only the diffraction lines from the steel itself were clearly distinguishable. The experiments performed with CoK_α radiation and an Fe filter for β lines gave much better results regarding the recording of surface oxide peaks. The low 2-theta angle region of the experimental X-ray diffraction patterns are presented in Fig. 1. The investigated angular region is chosen in this particular interval, enabling the measurement of only the oxide peaks, avoiding the possible overlapping with the set of peaks corresponding to the steel substrate (in the figure the only peak from the steel is the {1 1 0} line appearing at 2-theta ≈52°). The intensity of the diffraction lines covered a wide range so only the strongest lines are ev-

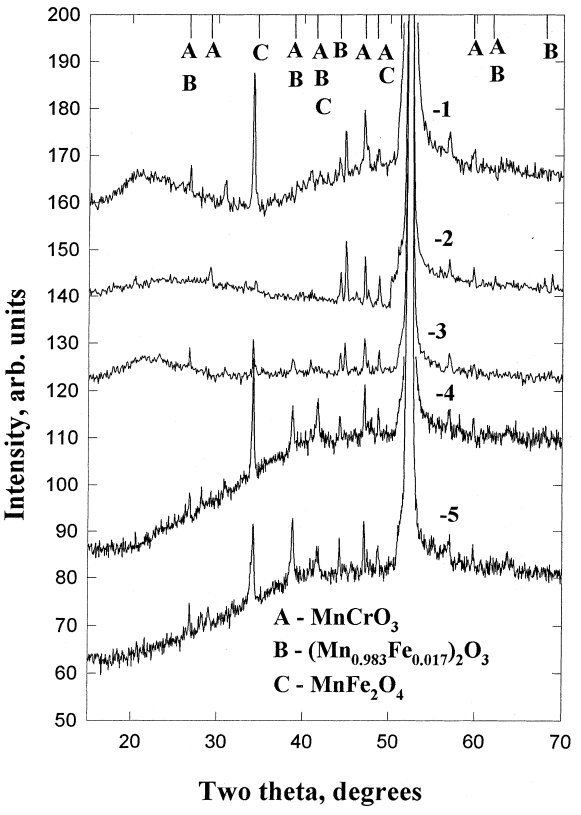

Fig. 1. X-ray diffraction patterns for the investigated samples, numbered 1–5. The identified diffraction lines are marked. The intense line at 2-theta≈52°, which occurs in all the patterns, is the {1 1 0} peak from the steel substrate.

ident in Fig. 1. Observation on a smaller intensity scale revealed the presence of more peaks, which were included in the qualitative phase analysis. In order to identify the existing phases, the measured diffraction patterns were compared to standard patterns for oxides of Fe, Cr, and Mn taken from the international powder diffraction files. A phase was assumed to be present if the positions of at least three lines were well matched with the standard patterns. However, no attempt was made to match the relative intensities of experimental and file patterns because of the expected presence of crystallographic texture in the investigated films. Following this method some or all of the following phases were identified in each of the samples:

(a) $(Mn_{0.983}Fe_{0.017})_2O_3$ – diffraction file No. 24-507, cubic symmetry;

(b) $MnCrO_3$ – diffraction file No. 26-1235, triclinic symmetry;

(c) $MnFe_2O_4$ – diffraction file No. 38-430, tetragonal symmetry.

As can be seen from Fig. 1, the experimental peaks were in some cases slightly shifted from the 'ideal' positions corresponding to the oxides above mentioned. This was thought to be due to the presence of a more complicated mixture of metal ions (i.e. Fe, Cr, Mn, Mo etc.) than is given in the above examples. However it could also be due to the existence of lattice defects in the grown oxide films or on the formation of residual stresses in the surface oxides during their growth and cooling. Thus, the surface oxides formed are complex: type (a) could be described with a general formula M_2O_3; type (b) is also of the form M_2O_3 but with a different crystal symmetry and type (c) is the manganese spinel $MnO{\cdot}Fe_2O_3$ (M_3O_4). In all these types, M represents a mixture of different metal atoms, which, in the above quoted powder diffraction files are respectively (Mn, Fe) for type (a); (Mn, Cr) for type (b) and (Mn, Fe) for type (c).

The qualitative phase analysis showed that in all the samples (except sample No. 2) all the three types of oxide phases have been formed. In sample No. 2, annealed in an atmosphere with a very low amount of oxygen, only oxides of types (a) and (b) have been revealed, no peaks corresponding to manganese spinel having been found at all.

X-ray qualitative analysis gave only information about the structural type of the oxides formed. The precise determination of the chemical composition of the surface oxides was carried out by the ion beam methods RBS and NRA. The RBS and NRA spectra are presented in Fig. 2. Fig. 2(a) shows the complete RBS spectra for samples No. 2 and No. 3 and Fig. 2(c) the NRA spectra for the same samples. It is obvious that on the scale of Fig. 2(a), the RBS spectra are similar in shape, consisting of a step corresponding to backscattering from surface metal atoms and a roughly level region due to collisions from underlying atoms. When the step region is looked at more closely as in Fig. 2(b) differences in shape between the spectra due to differences in the composition and thickness of the oxide layer are apparent. The greater atomic mass of Fe compared to Mn and Cr results in the alpha particles backscattered from surface Fe having a measurably higher energy than those backscattered from the other two atoms. Thus, variations in the relative amounts of metal atoms in the oxide changes the shape of the step of the spectrum. The energies at which the step would appear for surface Fe, Mn and Cr are marked on Fig. 2(b). If the oxide is thick enough and if there is a significant quantity of Fe in the oxide, the spectra has the shape of a double step (the higher energy one from the oxide and the other from the substrate), as revealed in the cases of Samples 3–5. In these spectra, the height of the first (higher energy) step is directly related to the quantity of Fe in the oxide and the width to the thickness of the oxide layer. The oxide film is so thin on Sample 1 that the first step cannot be easily distinguished and the shape of the spectrum is almost that which would be expected for a clean steel surface. However, the presence of an oxide on this sample was clearly evident from the NRA and X-ray diffraction results. In the case of Sample 2, the step appears at a lower energy than for the other samples, showing that the iron content of the oxide is low. In fact, the step occurs at an energy where backscattering from Mn is expected. It is notable that there is no obvious step at an energy corresponding to backscattering from Cr nuclei, suggesting that none of the samples contain a predominantly chromium-containing oxide phase.

The shapes of the NRA spectra are very similar for all the investigated samples. This is expected from the fact that this method is less sensitive for performing depth profiles compared to RBS. The intensity and the width of the peak depend on the thickness of the surface oxide layer (the higher and the broader the peak, the thicker the layer). Fig. 2(d) shows in one graph the O(d,p) peaks for all the investigated samples. It is obvious that the thickness of the formed surface oxide increases starting from sample No. 1 to sample No. 5 in the same sequence in which the samples have been numbered.

For the quantitative thickness and compositional determination the spectra have been fitted to simulated spectra as described previously. For all the samples, the fitting procedure started with the NRA spectra which gives a straightforward measure for the overall thickness of the surface oxides. As a guide for the initial estimation of the composition of the layer structure two sources were used: firstly, the phases revealed by the X-ray diffraction and secondly, typical layer structures from Refs. [6,8,9]. Then the parameters of chemical composition, layered structure and thickness have been improved by an accurate fit of the step and level region

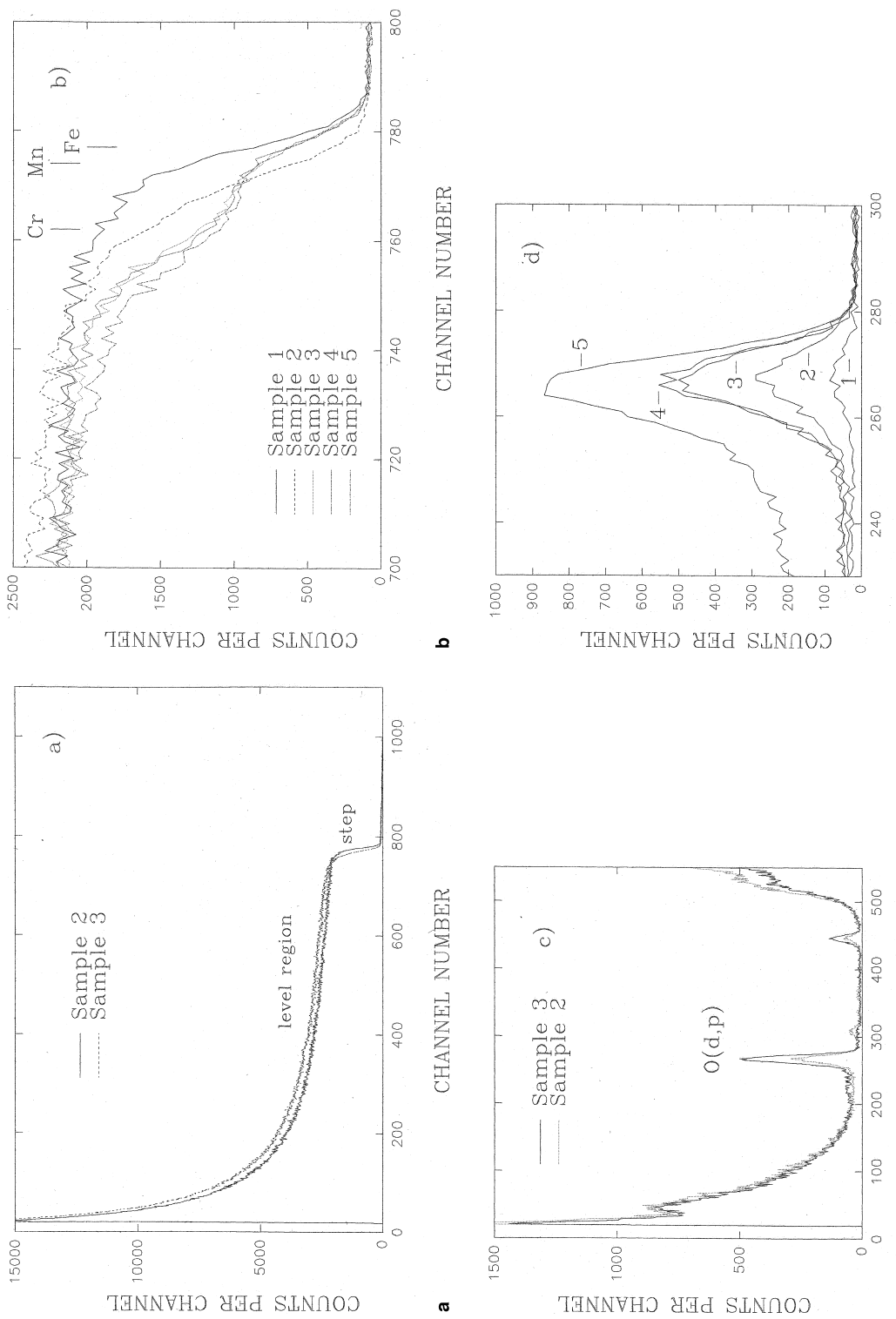

Fig. 2. Experimental RBS and NRA spectra: (a) a full RBS spectra for sample No. 2 and sample No. 3; (b) the step region of the RBS spectra for all the samples; (c) a full NRA spectra for samples No. 2 and No. 3 with marked O(d,p) peak; (d) the experimental O(d,p) peaks for all the samples.

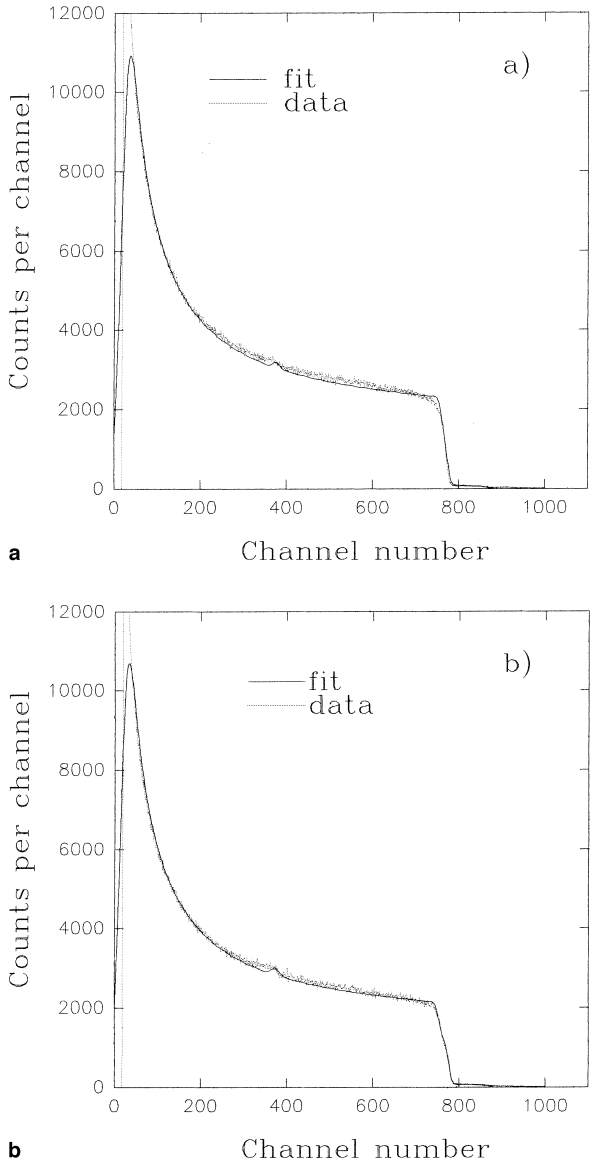

Fig. 3. Step regions of the experimental (solid line) and fitted (dotted line) RBS spectra: (a) for sample No. 2; (b) for sample No. 3.

of the RBS spectra. Fig. 3 presents in one graph the step regions of the experimental and fitted RBS spectra for sample No. 2 (Fig. 3(a)) and No. 3 (Fig. 3(b)). Similar fits were performed for all the samples. According to the fits, the oxides were complex (including Fe, Cr, Mn and Mo) and the samples annealed in air could be represented by a layered structure containing three compound oxide phases formed on the base of the crystal lattices of the three above mentioned basic oxide phases described by the formulae M_2O_3 and M_3O_4. The introduction of a monophase layer of pure Cr_2O_3 did not give satisfactory fits for any of the investigated samples. The chemical compositions and thickness of the oxide layers which form the total structure of the surface oxide films are given in Table 2. The theoretical (stoichiometric) number densities of the metal and oxygen ions in the lattices of the base oxides whose crystallographic structure is identical to the structure of the formed complex oxides are given in Table 3.

Thus, from the performed analyses it follows that the overall structure of the formed surface oxides could be represented as built-up by two or three monophase compound oxide layers whose thickness and composition depend on the conditions of oxidation. The macrostructure of the formed oxide films is schematically represented in Fig. 4. It is interesting to compare the

Table 2
Concentration of elements in the oxide layers and their thickness, d, as given by the RBS analysis

Sample no.	Concentration of elements $\times 10^{22}$ (at/cm^3)																	
	Layer 1 (outer)						Layer 2 (intermediate)						Layer 3 (inner)					
	Fe	Mn	Cr	Mo	O	d, nm	Fe	Mn	Cr	Mo	O	d, nm	Fe	Mn	Cr	Mo	O	d, nm
1	2.29	1.4	0.2	0.02	5.92	3.0	2.4	1.3	0.25	0.03	5.2	4.5	0.43	2.8	0.9	0.07	6.3	4.5
2	0.1	3.4	0.1	0.04	5.8	32	no intermediate layer					–	0.43	2.8	0.9	0.07	6.3	5.0
3	2.29	1.4	0.2	0.02	5.92	40	2.4	1.3	0.25	0.03	5.2	5.0	0.43	2.8	0.9	0.07	6.3	5.0
4	2.29	1.4	0.2	0.02	5.92	42	2.4	1.3	0.25	0.03	5.2	5.0	0.43	2.8	0.9	0.07	6.3	5.0
5	1.9	1.3	0.05	0.02	5.92	55	2.4	1.3	0.25	0.03	5.2	5.0	0.43	2.8	0.9	0.07	6.3	5.0

Table 3
Theoretical (stoichiometric) number densities of ions in the lattice of the base oxides

Oxide	Number density $\times 10^{22}$ (at/cm^3)	
	Metal ions	Oxygen ions
M_2O_3 (triclinic)	4.2	6.3
M_3O_4	3.9	5.2
M_2O_3 (cubic)	3.95	5.92

results obtained here with the standard models of oxidation of stainless steels as described previously. The obvious difference is that no pure Cr_2O_3 layer was formed at the metal/oxide interface. Instead, there is evidence for a complex oxide layer in which manganese is the predominating element. On the top of this, in the air oxidised samples, a spinel is formed, as the standard view predicts, but it is a Mn–Fe spinel ($MnFe_2O_4$) rather than an Fe–Cr spinel ($FeCr_2O_4$). The outermost layer for the air oxidised samples is predominantly iron oxide but with a substantial Mn content. In sample 2, oxidised in hydrogen, the spinel phase has not been formed and top layer is highly enriched with Mn but has little iron and chromium. From the data in Table 2 it also follows that for sample No. 2 the concentration of oxygen in both the surface layers which form the structure of the oxide film is less than the stoichiometric value (see Table 3). This is probably due to the very low concentration of oxygen in the annealing hydrogen atmosphere, which leads to the formation of oxygen vacancies in the grown oxide film. Also the top layer (layer No. 1) in sample No. 5, which has the thickest oxide film, contains a decreased concentration of metal ions which points out the existence of some cation vacancies in this layer.

In most of the stainless steels investigated in the papers referred to above [8,9,11], the Cr content is around 16% (or higher) and thus the formation of passivating surface oxides is controlled by this element. However, it appears that in MANET steel, which contains somewhat less chromium (around 10%), it is the highly mobile Mn atoms rather than Cr that tend to combine with iron and oxygen to form the oxide films when oxidised in air. In hydrogen, where the oxygen potential is low, the Mn content completely dominates the oxide film which has relatively small amounts of iron or chromium (the ΔG for oxidation of manganese is more negative than for Fe or Cr).

It is considered [6] that the kinetics of growth of surface oxides in iron during annealing obey the parabolic law $d \propto \sqrt{t}$ within the interval 200–1000°C and the logarithmic law $d \propto \ln(t)$ when the oxidation is per-

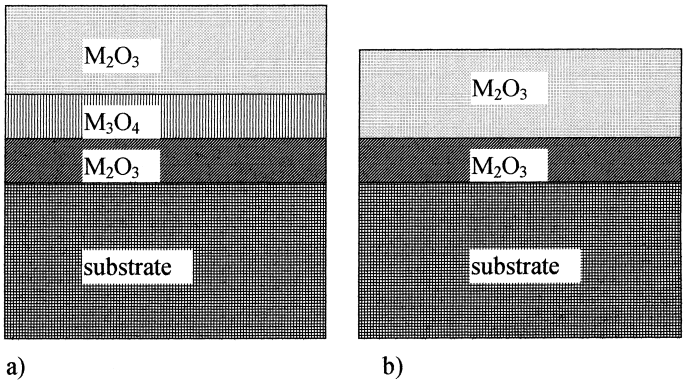

Fig. 4. A scheme representing the layered structure of the oxide films: (a) for samples oxidised in air; (b) for samples oxidised in hydrogen.

Table 4
Experimental and theoretical values of the total thickness (d) of the oxide films as a function of the annealing time (t) for the samples that were isothermally annealed at 600°C in air

Sample no.	Thickness (nm)	Thickness normalised with the thickness of sample No. 3	
		Experimental	Theoretical ($d \propto \sqrt{t}$)
3	50	1.00	1.00
4	52	1.04	1.41
5	65	1.30	3.46

formed at temperatures up to 200°C (where d is the oxide film thickness and t is the annealing time). Table 4 presents the comparison of the experimental thicknesses of the oxide films for the samples annealed in air at 600°C with the predicted thicknesses if a parabolic law is obeyed from $t = 0$ (data normalised to the thickness of Sample No. 3). It can be seen that the total thickness of the oxide film formed in the steel has increased by a factor of 1.3 when the annealing time has increased from 10 min to 2 h, a value that is much less than the predicted value of 3.49. Thus, from the limited amount of data available, it appears that in the case of MANET, the kinetics of formation do not follow a simple growth law over the entire oxidation process observed (i.e from time $t = 0$). Oxidation only follows a simple parabolic law if the diffusivity of the mobile ion species remains almost constant during the oxidation procedure. The existence and development of two or three monophase layers with different structure and composition in the oxide film will alter the diffusivity of metal ions from the substrate to the top of the growing oxide film thus changing the kinetics of growth. The results suggest that during the oxidation of the investigated high chromium martensitic steel, the diffusivity of the metallic ions that form the oxide film decreases during the growth of the coating.

5. Conclusions

1. During the oxidation of MANET steel in air at ambient temperature and at 600°C a mixture of compound surface oxides is formed. The structure of the total oxide film could be described by three layers in the following sequence starting from the steel surface: M_2O_3 (triclinic unit cell), M_3O_4 (spinel), M_2O_3 (cubic unit cell), where M is a mixture of Fe, Cr, Mn and Mo.

2. The annealing of the steel at 600°C in purified hydrogen (low oxygen potential) also causes surface oxidation and the formed film could be represented by a two-layered structure formed by the two oxides mentioned in point 1 above, described by the formulae M_2O_3, in which the crystal structures of the oxides contain oxygen anion vacancies. No spinel layer was formed in this case.

3. In all cases, the oxides formed were enriched with Mn relative to Fe and Cr (at least with respect to the concentration of these elements in the steel). This was especially evident for the sample heat treated under hydrogen where Mn was the predominant metal ion in the oxide film.

4. The kinetics of surface oxide growth in MANET steel annealed isothermally at 600°C in air do not follow a simple parabolic law over the entire oxidation period, which is probably due to the formation, by diffusion and chemical reaction, of monophase layers, which alter the growth characteristics of the whole film.

References

[1] M. Dalle Donne, D.R. Baskes, G. Kalinen, R. Mattas, S. Mori, J. Nucl. Mater. 215 (1994) 69.
[2] K.S. Forcey, D.K. Ross, J.C.B. Simpson, D.S. Evans, J. Nucl. Mater. 160 (1988) 117.
[3] K.S. Forcey, D.K. Ross, L.G. Earwaker, Z. Phys. Chem. 143 (1985) 213.
[4] W.A. Swansiger, R. Bastasz, J. Nucl. Mater. 85/86 (1979) 335.
[5] W.F. Smith, in: Structure and Properties of Engineering Alloys, Materials Science Engineering Series, McGraw-Hill, New York, 1981.
[6] R.E. Smallman, Modern Physical Metallurgy, 3rd ed., Butterworths, London, 1970.
[7] R.E. Reed-Hill, R. Abbaschian, Physical Metallurgy Principles, 3rd ed., PWS, Boston, 1991.
[8] I. Saeki, H. Konno, R. Furuichi, Corros. Sci. 38 (1996) 19.
[9] B. Chattopadhyay, G.C. Wood, Oxid. Met. 2 (1970) 373.
[10] R.E. Lobnig, H.P. Schmidt, K. Hennesen, H.J. Grabke, Oxid. Met. 37 (1992) 81.
[11] D. Abida, M. Lenglet, J. Lopitaux, C. Berthier, J.M. Lameille, E. Bencher, Proceedings of ECASIA'95, Montreux, Wiley, Chichester, 1996, 176.
[12] A. Perujo, S. Alberici, J. Camposilvan, F. Reiter, Fusion Technol. 21 (1992) 800.
[13] L.G. Earwaker, V. Piddock, J.M. Cole, J.C.B. Simpson, Nucl. Instr. and Meth. B 15 (1986) 367.
[14] J.C.B. Simpson, L.G. Earwaker, Nucl. Instr. and Meth. B 15 (1986) 502.